Title:

A high-throughput multiplex array for antigen-specific serology with automated analysis.

Rosenberg, A.F.[1,2], Killian, J.T. Jr. [4], Green, T.J.[1], Akther, J.[3], Hossain, M.E.[3], Shang, Q., Qiu, S[1]., Guang, Y.[1], Randall, T.D.[3], Lund, F.E.[1], and King, R.G.[1*]

Affiliations:

[1]Department of Microbiology, University of Alabama at Birmingham (UAB), Birmingham, AL 35294, USA

[2]Informatics Institute, UAB, Birmingham, AL 35294, USA

[3]Department of Medicine, Division of Clinical Immunology and Rheumatology, UAB, Birmingham, AL 35294, USA

[4]Department of Surgery, UAB, Birmingham, AL 35294, USA

*Corresponding author: rgking@uab.edu

Abstract.

High-throughput customizable CBA automated script-based analysis.

The utility of high-throughput systems to evaluate antigen-specific antibody (Ab) has been highlighted by the SARS-CoV-2 pandemic. Pathogen-specific Ab levels are often used to assess protection following vaccination and, in the case of novel pathogens, an indication of prior exposure. Several platforms exist to visualize antigen-specific Ab, however most are not quantitative and are difficult to scale for population level studies. Additionally, the sensitivity across platforms differs making direct comparisons between studies difficult. Cytometric bead arrays (CBA) are an attractive platform for antigen-specific Ab measurements as they can be used to assess Ab reactivity against several antigens and of several isotypes to be performed simultaneously. Additionally, CBAs exhibit high sensitivity and can be designed to provide quantitative measurements. Using commercially available particles, a biotin-Streptavidin bead loading strategy, and the inclusion of indirect standards, we describe a flexible system that can be modified to include a variety of antigens. Here we describe two arrays, focused on antigens derived from either β-coronaviruses or influenza virus. To support the high-throughput capacity of this system, we developed a suit of automated software tools, the CBA Toolbox, to process raw data into antigen-reactive IgM, IgA, and IgG concentrations. We describe quality control requirements, assay performance, and normalizations to accurately quantitate antigen-specific Ig.

1. Introduction

Pathogen-specific serum antibody (Ab) levels are commonly used to determine prior exposure history, to measure vaccine responsiveness, and to predict whether someone who was previously infected or vaccinated will be protected from reinfection. The COVID pandemic has highlighted the need for rapid and accurate quantification of antigen-specific Abs in human biologic samples. Early in 2020, the human immune response to SARS-CoV-2 was uncharacterized and considerable effort was devoted to determining how individuals respond to infection and whether particular Ab responses correlated with disease outcomes. Even following the approval of multiple SARS-CoV-2 vaccines, it was still unclear which serological features of the humoral immune response afforded protection against infection or re-infection with SARS-CoV-2. Unfortunately, the evolution of the Sars-2-CoV-2 pandemic over the last three years has illuminated the shifting landscape of viral variants and the uneven protection afforded by the original vaccination formulations [1, 2]. Despite numerous published large cohort studies [3-6] that addressed the magnitude and longevity of SARS-CoV-2 humoral immunity, it is clear that there is still a need to develop inexpensive, high-throughput methodologies to evaluate Ab responses following infection or vaccination [7, 8]. Additionally, it is now increasingly obvious that not all Abs directed toward the SARS-CoV-2 spike protein (C SP) are protective and that we need quantitative Ab detection platforms that can measure multiple isotypes of C SP Abs and can assess C SP Ab specificity for Spike variants and sub-domains of C SP. Although several platforms to detect SARS-CoV-2-reactive Abs [9-16] have been described, few of these platforms provide quantitative data. Thus, cohort data, which was generated using the different Ab platforms, cannot be directly compared across studies. This limitation has hampered our ability to define specific concentrations of C SP reactive Abs that correlate with protection. Such quantitative analyses are becoming increasingly important as SARS-CoV-2 variants that are resistant to prior vaccine responses continue to emerge [2]. Additionally, there are very limited open-source, non-instrument-linked options for automated analysis that would be suitable for high-throughput, batched Ab reactivity profiling [17]. Although the COVID pandemic has increased our appreciation for the utility of platforms that can be used to evaluate antigen-

74 specific Ab, such platforms are important for many other pathogens including seasonal
75 influenza (INF) virus. To address this need, we developed a highly customizable
76 cytometric bead array (CBA) platform to quantitate specific Abs of IgG, IgM, and IgA
77 subclasses against several pathogen associated antigens. Coupled with an automated
78 MATLAB analysis pipeline, the CBA Toolbox that is highly configurable like the assay
79 itself, this system allows for the high-throughput quantification of Abs reactive to a wide
80 variety of antigen panels.

81 CBAs have been widely employed to determine the concentration of diverse
82 analytes from biological samples, including Abs [18]. CBAs offer several advantages over
83 traditional ELISA-based approaches including enhanced sensitivity and a broad dynamic
84 range. In addition, CBA ligands can be multiplexed, thereby allowing for analysis of many
85 antigens simultaneously in a high-throughput format [14, 18].

86 Here we describe development of a highly customizable CBA platform that, when
87 coupled with automated MATLAB analysis pipeline, can be used in a high-throughput
88 manner to rapidly quantitate IgG, IgM, and IgA Abs specific for a variety of pathogen-
89 derived antigens. One CBA consisted of 12 antigens derived from β-Coronavirus (β-CoV)
90 virus spike ectodomains (SP) and nucleocapsid proteins (NP). The second array
91 incorporated 14 INF hemagglutinins (HA) in addition to influenza NP and non-structural
92 protein 1 (NS1). To support this detection platform, we developed a post-acquisition,
93 MATLAB-based analytic pipeline that allowed for streamlined data analysis and enabled
94 high-throughput use. In addition, we evaluated the performance of the array using panels
95 of monoclonal and polyclonal human Abs. Using these reagents, we determined antigen-
96 specific correction factors allowing for the accurate quantification of serum Ab of the IgM,
97 IgA, and IgG subclasses toward each of the array antigens. Although the configuration of
98 the arrays described here was focused on β-CoV- and INF-derived antigens, the platform
99 is flexible and utilizes indirect standards, which allow for quantitation of Ab reactivity to
100 essentially any protein antigen.
101

102 **2. Material and methods**

103 2.1 *Array generation*.

104 Streptavidin (SA) (SouthernBiotech 7105-01) was buffered exchanged into PBS using
105 PD-10 columns (Cytiva 17085101) and then diluted to 2mg/mL. SA was then conjugated
106 to spherotech 4μm and 5μm Carboxy Blue Particle Array Kits (Spherotech CPAK-4067-
107 8K and CPAK-5067-10K) using 1-Ethyl-3-(3-dimethylaminopropyl)carbodiimide (EDC)
108 chemistry. For conjugation, 1e8 spherotech particles were isolated by centrifugation at
109 10,000Xg for 3 min. After carefully removing the supernatant, the bead pellet was
110 resuspended in 0.5 mL SA in PBS. Following complete resuspension by pipetting, 0.5 mL
111 of 6mM EDC, dissolved in 0.05M MES buffer pH 5.0, was added, and the reaction mixture
112 was rotated at room temperature (RT) overnight (O/N). After the conjugation reaction was
113 complete, 0.1 mL 1M tris pH 8.0 was added to quench the reaction. Following a 1 hr
114 incubation, the beads were harvested by centrifugation as described above and washed
115 twice in 1mL PBS. Following the final wash, beads were resuspended at 10e8
116 particles/mL in PBS with 0.25% NaN3 and stored at 4ºC.
117 Following SA conjugation, quality control experiments were performed to
118 determine the degree and uniformity (when multiple particle sizes and/or peak identities
119 are used) of labeling by staining the SA-conjugated particles with Alexa488- labeled-
120 biotinylated hemagglutinin (HA) from the H1 HA derived from influenza A/PR/8/34 (PR8).
121 Individual array constituents were mixed and diluted to 1e6 of each particle/mL. 40 μL of
122 serial dilutions of PR8 HA were prepared in a 96 well U bottom plate (Corning 3797)
123 ranging from 1μg/mL to 2ng/mL. 5μL of the bead suspension was added, mixed by
124 pipetting, and incubated for 15 min at RT. 200μL PBS was added and the plate was
125 centrifuged at 3000Xg for 5min. The beads were resuspended in 80μL PBS. PR8 HA
126 bound to SA conjugated beads was visualized by flow cytometry.
127 Following SA coupling and quality control analyses described above, biotinylated
128 recombinant antigens were passively absorbed onto the individual particles. For antigens
129 described here (Table 1), a single biotin was added enzymatically onto a carboxy terminal
130 AVI tag. SA conjugated particles were harvested by centrifugation as described above
131 and resuspended in 1mg/mL of the recombinant proteins in 1% BSA in PBS. Antigen
132 loading was carried out by rotating overnight at 4ºC. Following absorption, the beads were
133 harvested by centrifugation as described, and washed twice with 1% BSA in PBS. Finally,

134 the antigen coated beads were resuspended at 1e8 particles/mL 1% BSA in PBS, 0.25%
135 NaN3 and stored at 4ºC until used.
136
137 *2.2 Recombinant antigens.*
138 *Production of pre-fusion recombinant Spike (SP) proteins.* Ectodomain SP pre-fusion
139 trimers (SARS-CoV-2 $S_{14-1211}$) were produced by co-transfecting plasmids encoding SP-
140 AviTag and SP-6X-HisTag constructs into FreeStyle 293-F Cells at a 1:2 ratio.
141 Transfected cells were cultured in FreeStyle 293 medium for 3 days and recombinant SP
142 trimers were purified from culture supernatant by FPLC using Nickel-affinity
143 chromatography. Purified proteins were biotinylated *in vitro* using BirA enzyme.

144 *Production of SP subdomains*. NTD (SARS-CoV-2 SP_{14-305}) and RBD (SARS-CoV-2
145 $SP_{319-541}$) monomers with a C-terminal dual AviTag/6X-HisTag sequence were produced
146 by transfecting single plasmid constructs into FreeStyle 293-F Cells. Following a 3-day
147 expression, subdomains were purified from culture supernatant by FPLC using nickel-
148 affinity chromatography and biotinylated by addition of BirA.

149 *Production of CoV nucleocapsid protein (N).* Recombinant N containing the full-length N
150 and tandem AviTag/6X-HisTag sequence was produced by co-transforming Rosetta cells
151 with the N expression plasmid and an inducible BirA expression plasmid. Bacterial
152 cultures were grown in the presence of chloramphenicol, ampicillin, and streptomycin,
153 induced with IPTG and supplemented with biotin. Biotinylated N protein was purified by
154 FPLC using a nickel-affinity column and subsequent size exclusion chromatography.

155 *Recombinant influenza HA protein production*. The nucleic acid sequence corresponding
156 to amino acids 18-524 of influenza HA ectodomains were synthetized (GeneArt,
157 Regensburg, Germany) for influenza virus strains listed in Table 1, as previously
158 described [19]. Synthetic constructs were cloned into the pCXpoly(+) vector modified with
159 a human CD5 leader sequence and a GCN4 isoleucine zipper trimerization domain
160 (GeneArt) followed by either a 6XHIS tag (HA-6XHIS construct) or an AviTag (HA-AviTag
161 construct). The HA–6XHIS and HA–AviTag constructs for each HA were co–transfected
162 using 293Fectin Transfection Reagent into FreeStyle™ 293–F Cells (ThermoFisher
163 Scientific) at a 2:1 ratio. Transfected cells were cultured in FreeStyle 293 expression

164 medium for 3 days. The supernatant was cleared by centrifugation. Recombinant HA
165 molecules were purified from these culture supernatants by FPLC using a HisTrap HP
166 Column (GE Healthcare) and eluted with imidazole gradient. Purified proteins were
167 biotinylated *in vitro* using BirA enzyme.

168 *Production of influenza NP and NS1 proteins.* The coding sequence of NP from PR8 was
169 synthesized in frame with the coding sequence for a 15–amino acid biotinylation
170 consensus site [20] on the 3′ end (GeneArt). The modified NP sequence was cloned in
171 frame to the 6X-HisTag in the pTRC–His2c expression vector (Invitrogen). NP protein was
172 expressed in the BirA biotin ligase producing *E. coli* strain CVB101 (Avidity), purified by
173 FPLC using a HisTrap HP Column (GE Healthcare) and eluted with a 50–250 mM
174 gradient. The coding sequence for the influenza virus A/PR8/34 NS1 gene (amino acids
175 3–230, Accession Number: AAA43536) was chemically synthesized (GeneArt) in frame
176 with a 3' addition of the coding sequence for the BirA enzymatic biotinylation consensus
177 site and the 6X-HisTag. Two mutations, R38A and K41A, demonstrated to prevent
178 aggregation of NS1 at high concentrations, were introduced into the NS1 gene by site-
179 directed mutagenesis. The recombinant NS1 gene was cloned into the pTRC–His2c
180 expression vector (Invitrogen) and expressed in the BirA-enzyme containing *E. coli* strain
181 CVB101 (Avidity). Biotinylated recombinant NS1 was purified by FPLC using a HisTrap
182 HP Column (GE Healthcare), eluted with a 50–250 mM imidazole gradient, buffer
183 exchanged and concentrated.

184

185 *Antibodies and standards.*
186 IG bound to microparticles was detected using fluorescent goat polyclonal anti-IG F(ab')2
187 secondaries, SouthernBiotech (IgM cat 2022-02, IgG cat# 2062-09, IgA cat# 2052-09).
188 Isotype standards were generated by performing the array on mixtures of IG capture
189 beads with 0.75x serial dilutions of purified human Abs SouthernBiotech (IgG cat# 0150-
190 01, IgM Cat# 0158L-01, IgA cat#0155L-01) ranging from 1µg/mL to 1.3 ng/mL. Anti-SARS
191 Abs JTK137_H22 and JTK137_K6 were generated from the C SP-binding B cells derived
192 from a vaccinated donor. The C SP reactive Ab CR3022 was acquired from IDT Biologika.
193 C SP reactive Ab AHA001 was purchased from Sanyou Bio. HA-reactive Abs

194 (P52d7_K12, P52d7_I1, and P52d7_D20) were generated from HA-binding B cells from
195 a vaccinated donor [21].
196 Polyclonal anti-C SP reactive Ab was purified from the serum of a vaccinated donor
197 using affinity chromatography. Briefly, 0.5 mg of purified C SP trimers generated as
198 described above was conjugated to cyanogen bromide activated Sepharose (Cytica
199 17043001) following manufactures protocol. 10mL serum was diluted into 40mL PBS and
200 filtered using a 0.45µm syringe filter (Corning 431220). C SP conjugated Sepharose was
201 added and rotated overnight at 4ºC. Resin was collected by centrifugation (2000Xg
202 10min) and washed twice with 50 mL cold PBS. After the final wash, resin was loaded
203 into a disposable micro column (Pierce 89868) and 0.1M glycine pH 2.8 was used to elute
204 Ab (5 fractions, 200µl) into 25µl 1M tris pH 9.0. Eluted fractions were pooled and
205 concentrated by centrifugation through a 30K centrifugal filter (Millipore Sigma
206 UFC500324). Following concentration, samples were buffer exchanged into PBS using a
207 0.5mL Zeba desalting column (Fisher scientific PI87767) and quantitated.
208
209 *2.3 Assay protocol*
210 Serum samples were diluted into PBS (1/7150 for IgG detection, or 1/500 for IgM and IgA
211 detection) and 40ul was arrayed in 96 well u-bottom plates. A 5µl suspension containing
212 a mixture of each antigen-coated microparticles (5e5 beads per antigen). The
213 suspensions were mixed by pipetting and incubated for 15min RT. The beads were
214 washed with 200µl PBS and centrifuged (3000Xg 5min RT). The CBA particles were
215 resuspended in a secondary staining solution consisting of the appropriate anti-Ig
216 secondary diluted 1/400 in 1%BSA containing PBS. The suspension was incubated for
217 15min RT in the dark. The beads were washed with 200µl PBS and pelleted (3000Xg,
218 5min RT). The particles were resuspended in 80µl PBS and analyzed on a BD Cytoflex
219 flow cytometer in plate mode at sample rate of 100µl/min. Data collection was stopped
220 following acquisition of 75 µL of sample. Following acquisition, the resulting FCS files
221 were processed and analyzed.
222
223
224 *2.4 Automated analysis and software*

225 We developed the CBA Toolbox to automatically process FCS files to rapidly quantify the
226 antigen binding by serum polyclonal Abs or purified Ab samples. This software was
227 developed in Matlab (The Mathworks, Inc. Natick MA, USA) version R2020a on MacOS.
228 It requires the Statistics and Machine Learning Toolbox, the Curve Fitting Toolbox and
229 the Signal Processing Toolbox. Additionally, code from Matlab Central
230 (www.mathworks.com/matlabcentral/) public code repository was incorporated into this
231 program [22-25]. This software is available on GitHub [https://github.com/UAB-
232 Immunology-Institute/cba-toolbox].
233
234 2.5 *Human serum samples.*
235 Human serum samples were collected from de-identified deceased organ donors.
236 Peripheral blood from human subjects was drawn into K2-EDTA tubes (BD Bioscience).
237 Plasma was isolated by density gradient centrifugation over Lymphocyte Separation
238 Medium (CellGro), aliquoted, and stored in LN_2. Cryopreserved samples were thawed at
239 RT and diluted 1/100 in PBS in a 96 well U bottom plate to generate a 'master plate'
240 stored at -20ºC. Final dilutions were generated in assay plates as needed. For initial
241 experiments focused on assay optimization and serum dilution determination, samples
242 were acquired from consented participants under the UAB Institutional Review Board
243 approved the study protocol (IRB-300005127).
244
245 **3. Results and discussion**
246 ***3.1 Generation of antigen loaded microparticles:***
247 To evaluate the possibility of using antigen loaded beads to quantitate specific Ig, we
248 adsorbed CA09 HA and C SP onto two distinct SA conjugated particles and stained each
249 with the I1 HA reactive and CR3022 C SP-reactive mAbs. The MFI of binding by these
250 two mAbs to their cognate antigen coated particles were nearly identical when tested at
251 100µg/mL to 1ng/mL concentrations (FIG 1a) demonstrating that the linear range of the
252 CBA array was nearly three orders of magnitude and that the assay could reproducibly
253 detect specific Abs at a concentration as low as 10ng/mL Additionally, the MFI curves as
254 a function of concentration were also nearly identical, suggesting that when antigen

255 loading is carefully controlled to be equivalent, the MFI signal is dependent on mAb
256 concentration irrespective of the antigen.

257 Because the derived MFI represents the association of the fluorescently labeled
258 secondary Abs with the bead:Ag:Ab complex it is independent of the nature of the
259 antigen, we therefore considering using beads coated with anti-Ig to allow quantification
260 of bead bound Ab. We generated IgG capture beads by absorbing biotinylated anti-
261 human IgG Fab(2) to the same lot of SA conjugated beads coated with HA and C SP.
262 We then incubated these reagents with additional mAbs specific for either C SP
263 (CR3022, AHA001, H22, and K6) or HA (K12, I1, and D20) and compared the MFIs
264 following staining with fluorescently conjugated anti-IgG secondaries.

265 As seen in Figure 1b, the MFI signals derived from both the antigen coated and Ig
266 capture conjugated beads were highly similar across the dilution range toward their
267 cognate antigen and exhibited little or no binding to their non-cognate beads. The MFI
268 Ag/Ig bead ratio differed slightly among mAbs likely reflected differences in the affinity of
269 these mAbs for their cognate antigen, as has been described for these HA reactive Abs
270 [21]. These data confirm that biotinylated anti-isotype capture Abs, when the antigen
271 density and capture Abs on the beads was equivalent, mirror the quantity of antigen
272 bound Ig and serve as an indirect standard for antigen reactive Ab quantification.

273

274 *3.1 Generation of the β-COV and INF arrays.*

275 To simultaneously interrogate Ab reactivity to multiple viral protein antigens, we expanded
276 this array to include all particles available in the 4um and 5um kits which have distinct
277 inherent fluorescence in the far-red channels (FIG 2ab). We maximized SA conjugation
278 such that the binding capacity of each bead was high and uniform. To ensure equivalent
279 SA loading across bead sets, the biotin binding capacity was evaluated by incubating SA
280 bead preparations with an Alex-488 labeled recombinant influenza A/PR/8/34
281 hemagglutinin (PR8 HA) trimer that was biotinylated at a single site on the C-terminus of
282 the trimer (FIG 2b). As expected, the intensity of bead labeling by the fluorescent HA
283 trimer was dependent on the amount of HA protein in the reaction. Not surprisingly, the
284 4μm and 5μm particles exhibited different maximum intensities due to the difference of
285 surface area (therefore differences in total SA bound) between the two particles sizes

286 (FIG 1bc). However, SA loading was uniform when comparing particles of the same size,
287 with a coefficient of variation of 5.39% and 5.34% for all 5μm and 4μm beads,
288 respectively.

289 Next, we determined the biotin binding capacity of the SA-conjugated beads. First,
290 we incubated the SA-conjugated particles with an excess of a known amount of
291 biotinylated influenza HA trimers and measured the protein absorbed from these
292 suspensions using UV spectrometry. For the two independent lots of SA-conjugated
293 beads we tested, an average equivalent of 220μg HA protein per $1X10^8$ particles was
294 absorbed. Second, we incubated the SA beads with decreasing concentrations of
295 fluorescently labeled PR8 HA and determined the mean fluorescence intensity (MFI) of
296 binding (Fig. 2D). The point of inflection, at which the MFI of the beads progressively
297 diminished as a function of decreasing PR8 HA concentration indicating a sub-saturating
298 quantity of biotin, equated to the same value as determined by the first method –
299 specifically 200μg of PR8 HA per 1e8 beads. Based on these two approaches, we
300 estimated the typical biotin binding capacity of the SA beads to be 0.1 picomole
301 biotinylated protein per SA conjugated particle.

302 To generate antigen arrays, we absorbed recombinant viral proteins to the
303 individual fluorescent microparticles (Table 1). β-CoV array consist of full length, pre-
304 fusion stabilized SP trimers derived from the 5 known β-CoV: SARS-CoV-1 (S), SARS-
305 CoV-2 (C), MERS (M), HKU1 (H) and OC43 (O). In addition to the monomeric Receptor
306 binding domain (RBD) subunit of SP from SARS-CoV-1 and SARS-CoV-2 and the SP N-
307 Terminal Domain (NTD) from SARS-CoV-2. Finally, INF HA (CA09 HA) was included as
308 a positive control in the array as Abs specific for recently circulating INF strains or vaccine
309 constituents can be found in almost all adults.

310 For the INF array, we absorbed HA derived from 14 influenza viruses to
311 microparticles listed in Table 1b, in addition to INF NP and NS1. These HA represented
312 the most common circulating H1 and H3 strains over the last decade, as well as PR8, a
313 common laboratory strain, and a member of H2, H5, and H7 strains.

314

315 *3.4 Antibody standards and quantification:*

316 Although the data above suggested that the CBA could provide sensitive
317 qualitative assessment of antigen-specific Ab levels, we sought to refine the assay to
318 accurately measure the amount of antigen-specific Ab present in biological specimens.
319 We postulated that the relationship between Ab concentration and MFI derived from the
320 CBA analysis of these Abs would be dependent on several factors, including the Ab
321 isotype, which is unequally recognized by pan IgG secondaries, the affinity of the Ab for
322 the antigen, and the valency of Ab-antigen interactions. To normalize minor deviations
323 in biotin binding capacity between the individual array components, and the notable
324 differences between particle sizes, and we incorporated all individual particles into a
325 panel of Ig-capture beads distributing anti-IgM, -IgA, and -IgG capture beads across all
326 the beads used for the antigen arrays (FIG S1a). In parallel to the antigen specific array,
327 Ig capture bead mixtures were stained with purified IgM, IgA, or IgG serially diluted
328 (0.75x) from 1ug/mL to ~1ng/mL. The resulting standard curves were then used to
329 extrapolate the Ab isotype bound to the antigen-specific beads thus providing an
330 accurate quantification (FIG S1b).
331
332 *3.3 Assay functional range and dilution factor determination*
333 CBAs, just like conventional ELISAs, can exhibit prozone effects when the
334 concentration of the Abs being evaluated exceeds the binding capacity of the array.
335 Although prozone effects are less prominent in assays with a larger dynamic range, it is
336 still important to choose analyte dilutions that allow for accurate extrapolation of the MFI
337 measurements to concentration. This is particularly important for polyclonal sera
338 analyses. To identify a dilution range that would facilitate accurate measurements of viral
339 antigen specific IgG, IgM, and IgA serum Abs, we diluted (between 1/500 and 1/20517)
340 serum samples from ten SARS-CoV-2 convalescent patients and analyzed the samples
341 using the β-CoV CBA. As shown in Figure 3, the maximum MFI of binding by C-SP
342 reactive IgG Abs to the C-SP coated beads was significantly higher when compared to
343 maximum binding by C SP-specific IgA and IgM Abs. For samples that contained
344 detectable anti-C SP IgG, the prozone effect was apparent at dilutions below 1/7000, after
345 which the signal decayed as a function of Ab concentration. By contrast, IgM and IgA Abs
346 specific for C SP, which could be detected at a 1/7000 dilution in some samples, did not

347 exhibit a prozone effect at this dilution. This difference was likely due to the relatively
348 lower concentrations of C SP-specific IgA and IgM Abs present in serum [26] or to
349 differences in signal intensity, which is influenced by the isotype-specific secondaries.
350 Using this experiment as a guide, we determined that a 1/7100 dilution of convalescent
351 SARS-CoV-2 serum was appropriate to measure C SP-specific IgG while a 1/500 serum
352 dilution was appropriate to measure C SP-specific IgM/IgA. However, the appropriate
353 dilution of serum necessary to avoid prozone effects in the CBA must be empirically tested
354 and is likely to be dependent on the Ab levels within the experimental samples being
355 assessed and the antigen of interest.
356
357
358 *3.5 Automated Analytic Workflow*
359 Although the array data, which was collected as FSC files using a traditional flow
360 cytometer, could be analyzed using many different flow cytometric software packages,
361 the inclusion of multiple standard curves and the large number of individual flow files
362 made manual data processing laborious and subjective. To circumvent these issues we
363 developed a software pipeline to perform automated sample quality assessments and
364 batch processing. This software, written in Matlab (The Mathworks, Inc., Natick MA,
365 USA), processed individual raw FCS files to identify events associated with the beads, to
366 find bead peaks and to summarize the raw data. The software analyzed the standard
367 controls and automatically back-calculated concentration units from raw MFI data. The
368 software was also designed to work in batch mode, which allowed for processing many
369 files at once.
370 The overall workflow is shown in Figure 4. The command line program required
371 four arguments: (i) a directory containing all the FCS files; (ii) a sample manifest
372 containing metadata for each of the corresponding FCS files, including the flow cytometry
373 channel mappings for the bead channel and the secondary isotype channel; (iii) a
374 configuration file describing the association of bead peak order (numbered from lowest to
375 highest FL4 MFI) with protein for the specific assay, (iv) and a configuration file containing
376 parameters for peak identification. The output was a Matlab structure array where each
377 element contains a table of isotype reactivity for each feature (individual bead/isotype

MFI) in the assay as well as other program settings for complete analytical provenance supporting reproducibility.

This structure array, in turn was used for an analysis quality assessment program to visually summarize the consistency of the bead gates for each bead size as well as the numbers of beads for each bead gate as shown in Figure S2. This structure array was also used to generate standard curves for each isotype, bead size and sample dilution (multiple dilutions can be run together and are annotated in the sample manifest, and each requires their own set of standard curve samples). The samples used to generate the standard curves were annotated in the sample manifest. These data were used to compute a four-parameter logistic (4PL) fit for each bead size/isotype/dilution as shown in Figure S1b Finally, the structure array and the 4PL fits were used to back-calculate concentration units for the hyperbolic arcsine-transformed MFI data. The software program then outputs the entire data set to a single, tabular text file that was suitable for importing into any analysis program or relational database for large-scale studies. This software was also suitable for high-throughput use as data derived from five 96-well plates run on a Cytoflex (Beckman Coulter, Indianapolis IN, USA) – 480 samples including standards – could be processed in about a minute on a current model Macbook Pro laptop with no special memory or processor requirements.

3.6 Deriving MFI Reactivity Data from a Sample

The computational workflow was designed to parallel the process for manually quantifying the concentration of antigen-specific Abs in a sample (Figure 5). First, the MFI datapoints for each sample were extracted from the FCS files [22], transformed using a hyperbolic arcsine [23] and then visualized in a forward-scatter vs. side-scatter plot. The beads of different sizes (4um and 5um) were automatically detected by looking for the expected number of peaks along the forward-scatter (x) axis to define gates, and then, within each gate, to identify single peaks on the side-scatter (y) axis. The intersection of these gates in 2-D space was used to define oval gates (FIG 5a). Events that were present in each oval gate were annotated as distinct bead populations. Next, forward-scatter height vs. area plots for events in each bead gate were evaluated using density-based clustering and outliers, which represented non-singlet beads were then excluded (FIG 5b). Singlet

409 beads were then used for peak finding (for each bead size gate) based on transformed
410 MFI of the specified bead channel specified in the manifest header and compared against
411 the expected number of peaks as indicated in the array configuration file (FIG 5c). Finally,
412 events from each bead gate were evaluated on the secondary isotype flow channel(s)
413 specified in the manifest header to quantify the location of the peak (in transformed MFI)
414 for each bead feature and isotype (FIG 5d).
415 This software can accommodate an optional "split channel" prior to bead peak
416 detection (Figure 5c). By labeling half the beads prior to flow and employing an otherwise
417 unused flow channel to detect this signal, the number of antigens profiled can be
418 potentially doubled. Importantly, comparison of MFIs computed with the automated
419 software to manual processing using FlowJo (BD Biosciences, Franklin Lakes NJ, USA)
420 led to similar results, as shown in Figure S2 for four representative samples.
421
422 *3.7 Polyvalency and subunit corrections:*
423 When we began to analyze serum samples and polyclonal Ab preparations, we noted
424 that the highest MFI values observed often eclipsed that recorded using antigen-specific
425 mAbs, suggesting that the use of antigen-specific mAbs standards would result in an
426 overextrapolation of the total antigen-specific Ab in more complex samples, and that the
427 cytometric array is sensitive to effects resulting from the polyvalency of Abs present in
428 sera or other polyclonal Ab preparations. We hypothesized that multiple epitopes present
429 on antigens were simultaneously bound resulting in higher maximum MFI values than
430 exhibited by an equivalent concentration of a mAb, a phenomenon that would influence
431 Ab quantification. To determine if this were the case, and to quantitate this polyvalency
432 effect, we assayed a polyclonal C SP reactive Ab preparation derived from the serum of
433 a vaccinated donor. Using antigen-specific capture beads to quantitate the Ab isotype in
434 this preparation, we determine it was composed of 90 percent IgG, 10 percent IgA, with
435 low but detectable levels of IgM. Because IgA was present as a significant portion C SP
436 reactive Ig, we further purified IgG using protein G chromatography yielding an anti-C SP
437 pIgG with a mixture of IgG subclasses. We then evaluated both the pAb and IgG anti-C
438 SP preparations in the CBA. As can be seen in Figure 6a, the MFI of the IgG detection
439 Abs was noticeably but marginally higher in the IgG fraction resulting from the presence

440 of IgM and IgA Abs in the Ig preparation. We then used the array to quantitate C SP Abs
441 and compared these calculated values to the known concentrations. Although the
442 calculated values were higher than the known concentrations, they exhibited a linear
443 relationship up to concentrations of approximately 0.75 ug/mL, a concentration in which
444 the prozone effects of anti-SP Abs become apparent (FIG 6a). By comparing the known
445 IgG concentration with the calculated values along the serial dilutions within the linear
446 range we could determine the increase in apparent concentration resulting from the
447 polyclonality of the purified anti-C SP Ab, which was an apparent 3.16-fold inflation of the
448 calculated concentration (FIG 6b). These data demonstrate the average polyvalency
449 effect within the assay is constant within the range of concentrations indicated and
450 provided a correction factor for extrapolated Ig concentration values. To further confirm
451 this normalization was accurate, we assayed the NIBSC anti-C SP standards at serial
452 dilutions ranging from 1/1e3 to 1/8.65e4. When the resulting anti-C SP values are
453 corrected and plotted against the known dilutions of the pAb anti-C SP they collapse to
454 near identity, confirming the accuracy of this correction (FIG 6c). Using this approach, we
455 calculate the total anti-SP IgG to be 221.7μg/mL and 90.4μg/mL in the NISBC standards
456 2-/162 and 21/324 respectively (Fig 6d).
457 In addition to the polyvalency effects described above, we noted that the MFI values
458 were higher for the C RBD particles than for full-length SP trimers. This effect was
459 manifested as exceptionally high extrapolated anti-C RBD values in some samples.
460 Comparing the MFI of the C RBD and C SP beads resulting from staining with dilutions
461 of four RBD reactive mAbs, we consistently observed higher values for the RBD particles
462 (FIG 6e). As these Abs recognize an identical epitope on both antigens and the bead
463 constituents exhibit identical biotin binding capacity, we reasoned that because the RBD
464 is expressed as a monomer and has variable accessibility in the full-length trimers (RBD
465 up-down configurations [27]) the epitope density is unequal between these configurations.
466 To determine if this was a consistent effect, we analyzed the fold difference in MFI
467 between C SP and C RBD beads at a range of concentrations of four anti-RBD Abs (FIG
468 6f). Although the CBA signal derived from mAbs is dependent on Ab affinity in addition to
469 concentration, three of these Abs exhibit a concentration independent 1.5-fold increase

470 in C RBD MFI compared to that of C SP trimers, allowing us to correct for differences in
471 RBD epitope availability between full length SP and monomers.
472
473 *3.8 Sensitivity, accuracy, and reproducibility.*
474 Although the array results are highly reproducible when assaying monoclonal antigen-
475 specific Abs or isotype-specific Ab standards, we sought to determine the variance of
476 array across repeated measurements. To quantitate the reproducibility of the array
477 derived Ab values, we analyzed serum available through the UAB Comprehensive Center
478 for Human Immunology (CCHI) donor repository twice, independently, with COVID and
479 INF arrays. The MFI of each antigen in the arrays was nearly identical in the between the
480 two replicates (FIG 7a). Because acquisition for most of these samples pre-dated the
481 COVID19 pandemic, they did not contain detectable SARS-CoV-2 antigen reactivity (FIG
482 S3). However, IgG reactivity toward one or more HA antigens was observed in all
483 samples. The calculated value of the most prominently targeted HA antigens (including
484 both H1 and H3) were in close agreement between the replicates (FIG 7b). Although
485 deviations between replicates were noted at the highest Ab levels detected, these fall
486 outside of the linear range of the assay. Within the range of confidence, we observed a
487 high level of agreement between the two measurements. Importantly, as shown in Figure
488 7c, the calculated values of CA09 HA, which was included in the COVID array as a
489 positive control, were nearly identical in both arrays. As these reagents were generated
490 independently using different lots of SA beads, this demonstrates the reproducibility of
491 both bead generation and assay measurements.
492 To quantitate the reproducibility of the assay, we examined the mean absolute
493 deviation of IgG and IgA reactivity toward the three most frequently targeted HA H1 and
494 H3 antigens (FIG 7d). The average deviation is less than 5% across all these antigens,
495 and slightly lower for IgG (2.5%) than for IgA (4%). Collectively these data suggest the
496 arrays are highly reproducible both at the level of bead generation and in their
497 performance.
498 We did not observe Ab binding to C SP coated beads in serum samples collected
499 before the spring of 2021, despite IgG reactive with O SP being readily quantifiable in all
500 samples (serum antigen-specific Ab concentrations for all antigens is shown in Figure 8).

501 Following the spring of 2021, C SP reactivity was observed in 13/19 samples whereas C
502 NP reactivity was only observed in 4. In every case, C NP reactivity was corelated with C
503 SP Ab, suggestive of a prior infection (FIG S3). These data are consistent with the
504 infection and vaccination rates within the general population from which these donors
505 were derived [28].

506 Although HA reactivity was observed in all samples, there were significant
507 differences in the HA reactivity and Ab levels observed across individuals, representative
508 array histograms shown in Figure S4. A bias toward either H1 or H3 HA was observed in
509 some individuals, while others exhibited a balanced anti-HA Ab repertoire, although the
510 recent vaccine formulations were apparent, with CA09, Brisbane (H1) and MI15
511 demonstrated the highest level of reactivity. Reactivity toward PR8 was observed to be
512 the lowest of H1 HA (FIG 8). Reactivity toward H3 were generally lower than that of H1
513 while reactivity toward the H2, H5, H7 and H9 included in the array were rarely detected.
514 Most individuals exhibited IgG and IgM Abs toward INF NP while only 10% harbored
515 serum reactivity toward INF NS1, perhaps indicative of a recent INF infection. When we
516 compared the reactivity of these antigens, we noted a significant correlation between H1
517 and H3 HA, which were poorly correlated with one another (FIG 9a). Although we cannot
518 determine if this is due to cross-reactive Abs, or that similar levels of Abs that target these
519 antigens, high sequence similarity, as is the case for CA09 and MI15, are associated with
520 the highest correlation of Ab levels (FIG 9bc). Interestingly, although IgG and IgA Ab
521 levels are both highly corelated toward similar HA antigens, the IgG and IgA levels
522 themselves do not correlate (FIG 9cd), perhaps suggestive of different origins of HA
523 reactive Abs of these isotypes. Collectively these data demonstrate the assay is suitable
524 for high-dimensional, high-throughput Ab reactivity determination.
525

526 4. Conclusions

527 Here, we describe an CBA platform designed to conduct high-throughput determination
528 of Abs reactive with viral antigens. The assay provides a rich view of the humoral immune
529 landscape by multiplexing the analysis of 12 β-CoV or 16 INF antigens into a single assay.
530 By altering dilutions factors and secondary detection reagents, the levels of IgG, IgM, and
531 IgA can be accurately determined. This platform exhibits high sensitivity, although the

532 lower limit of detection is dependent on dilution factor, as little as 2ng/mL of antigen-
533 specific IgG in the final dilution can be measured. The assay demonstrates high
534 specificity, as demonstrated by multiple monoclonal Abs, the reactivity to each antigen in
535 the array is discrete. The use of multiple indirect standards provides accurate
536 quantification for Ab reactive to each antigen across all assayed isotypes. Additionally,
537 the assay requires minute amounts of both antigen and serum tested, typically consuming
538 less than 0.5μg of antigen and less than 1μL of sample per assay.

539 Although, the CBA array described here is focused on β-CoV and INF serology,
540 the same strategy can be implemented to evaluate serum Ab to a wide array of antigenic
541 targets. The use of recombinant antigens, like the various SP ectodomains and subunits
542 or HA and NP described here, allow for the rapid replacement or addition of similar
543 antigens into the CBA with no required modification to the analytics. Although the
544 corrections for polyvalency and subunit epitope availability are specific for C SP, these
545 are the product of the physical nature of the antigens included in the current array, and
546 whether such corrections are applicable to other antigens necessitates empirical
547 determination. Polyclonal corrections may be generalizable, however, the number of
548 individual Abs that may simultaneously bind their cognate antigen is influenced by
549 immunodominance of epitopes and steric hindrance, an idea supported by structural
550 studies [29-31].

551 The high-dimensional assay we described greatly benefits from the use of the
552 automated analytic platform. When combined, this system facilitates the rapid and
553 accurate determination of antigen reactive Ab. Although the source material used as
554 examples in this study are serum, the assay is amenable to many biological samples
555 including nasal washes and saliva. The capacity to visualize both the magnitude and
556 breadth of Ab responses to vaccination or infection with respiratory pathogens is valuable
557 in determining correlates of protection derived from vaccination or pathogen exposure,
558 and the ability to easily and rapidly expand the antigens incorporated into the array with
559 minimal effects on the established analytics makes this approach an attractive option to
560 fill the continuing need for large-scale serology studies.
561

562 1. Garcia-Beltran, W.F., et al., *Multiple SARS-CoV-2 variants escape neutralization by*
563 *vaccine-induced humoral immunity.* Cell, 2021. **184**(9): p. 2372-2383 e9.
564 2. Yadav, P.D. and S. Kumar, *Global emergence of SARS-CoV-2 variants: new foresight*
565 *needed for improved vaccine efficacy.* Lancet Infect Dis, 2022. **22**(3): p. 298-299.
566 3. Aldridge, R.W., et al., *SARS-CoV-2 antibodies and breakthrough infections in the Virus*
567 *Watch cohort.* Nat Commun, 2022. **13**(1): p. 4869.
568 4. Alfego, D., et al., *A population-based analysis of the longevity of SARS-CoV-2 antibody*
569 *seropositivity in the United States.* EClinicalMedicine, 2021. **36**: p. 100902.
570 5. Hall, V.J., et al., *SARS-CoV-2 infection rates of antibody-positive compared with antibody-*
571 *negative health-care workers in England: a large, multicentre, prospective cohort study*
572 *(SIREN).* Lancet, 2021. **397**(10283): p. 1459-1469.
573 6. Wang, Z., et al., *mRNA vaccine-elicited antibodies to SARS-CoV-2 and circulating variants.*
574 Nature, 2021. **592**(7855): p. 616-622.
575 7. Meyer, B., C. Drosten, and M.A. Muller, *Serological assays for emerging coronaviruses:*
576 *challenges and pitfalls.* Virus Res, 2014. **194**: p. 175-83.
577 8. Pisanic, N., et al., *COVID-19 Serology at Population Scale: SARS-CoV-2-Specific Antibody*
578 *Responses in Saliva.* J Clin Microbiol, 2020. **59**(1).
579 9. Caceres-Martell, Y., et al., *Single-reaction multi-antigen serological test for comprehensive*
580 *evaluation of SARS-CoV-2 patients by flow cytometry.* Eur J Immunol, 2021. **51**(11): p.
581 2633-2640.
582 10. Cameron, A., et al., *A Multiplex Microsphere IgG Assay for SARS-CoV-2 Using ACE2-*
583 *Mediated Inhibition as a Surrogate for Neutralization.* J Clin Microbiol, 2021. **59**(2).
584 11. Dawson, E.D., et al., *Multiplexed, microscale, microarray-based serological assay for*
585 *antibodies against all human-relevant coronaviruses.* J Virol Methods, 2021. **291**: p.
586 114111.
587 12. Egia-Mendikute, L., et al., *Sensitive detection of SARS-CoV-2 seroconversion by flow*
588 *cytometry reveals the presence of nucleoprotein-reactive antibodies in unexposed*
589 *individuals.* Commun Biol, 2021. **4**(1): p. 486.
590 13. Guarino, C., et al., *Development of a quantitative COVID-19 multiplex assay and its use for*
591 *serological surveillance in a low SARS-CoV-2 incidence community.* PLoS One, 2022. **17**(1):
592 p. e0262868.
593 14. Jolley, M.E., et al., *Particle concentration fluorescence immunoassay (PCFIA): a new, rapid*
594 *immunoassay technique with high sensitivity.* J Immunol Methods, 1984. **67**(1): p. 21-35.
595 15. Kenny, G., et al., *Performance and validation of an adaptable multiplex assay for detection*
596 *of serologic response to SARS-CoV-2 infection or vaccination.* J Immunol Methods, 2022:
597 p. 113345.
598 16. Roy, D.R., et al., *Development, Validation, and Utilization of a Luminex-Based SARS-CoV-*
599 *2 Multiplex Serology Assay.* Microbiol Spectr, 2023: p. e0389822.
600 17. Stervbo, U., T.H. Westhoff, and N. Babel, *beadplexr: reproducible and automated analysis*
601 *of multiplex bead assays.* PeerJ, 2018. **6**: p. e5794.
602 18. Morgan, E., et al., *Cytometric bead array: a multiplexed assay platform with applications*
603 *in various areas of biology.* Clin Immunol, 2004. **110**(3): p. 252-66.
604 19. Allie, S.R., et al., *The establishment of resident memory B cells in the lung requires local*
605 *antigen encounter.* Nat Immunol, 2019. **20**(1): p. 97-108.

606 20. Beckett, D., E. Kovaleva, and P.J. Schatz, *A minimal peptide substrate in biotin holoenzyme*
607 *synthetase-catalyzed biotinylation.* Protein Sci, 1999. **8**(4): p. 921-9.
608 21. Nellore, A., et al., *A transcriptionally distinct subset of influenza-specific effector memory*
609 *B cells predicts long-lived antibody responses to vaccination in humans.* Immunity, 2023.
610 22. fca, B.L. *readfcs.m* balkay.laszlo@med.unideb.hu, Department of Medical Imaging,
611 University of Debrecen. Version 22/Jun/2020. Matlab File Exchange. 2020; Available from:
612 https://www.mathworks.com/matlabcentral/fileexchange/9608-fca_readfcs.
613 23. Finak, G., et al., *Optimizing transformations for automated, high throughput analysis of*
614 *flow cytometry data.* Bmc Bioinformatics, 2010. **11**.
615 24. G., C. *L4P.m, Four parameters logistic regression - There and back again (2012)*. Matlab
616 File Exchange. 2012; Available from:
617 https://it.mathworks.com/matlabcentral/fileexchange/38122.
618 25. R., H. *Flow Cytometry Data Reader and Visualization* 2021; Available from:
619 https://www.mathworks.com/matlabcentral/fileexchange/8430-flow-cytometry-data-
620 reader-and-visualization.
621 26. Gaebler, C., et al., *Evolution of antibody immunity to SARS-CoV-2.* Nature, 2021.
622 **591**(7851): p. 639-644.
623 27. Henderson, R., et al., *Controlling the SARS-CoV-2 spike glycoprotein conformation.* Nat
624 Struct Mol Biol, 2020. **27**(10): p. 925-933.
625 28. Health, A.D.o.P. *Coronavirus Disease 2019 (COVID-19)*. 2023; Available from:
626 https://www.alabamapublichealth.gov/covid19/.
627 29. Barnes, C.O., et al., *Structures of Human Antibodies Bound to SARS-CoV-2 Spike Reveal*
628 *Common Epitopes and Recurrent Features of Antibodies.* Cell, 2020. **182**(4): p. 828-842
629 e16.
630 30. Nogal, B., et al., *Mapping Polyclonal Antibody Responses in Non-human Primates*
631 *Vaccinated with HIV Env Trimer Subunit Vaccines.* Cell Rep, 2020. **30**(11): p. 3755-3765
632 e7.
633 31. Han, J., et al., *Polyclonal epitope mapping reveals temporal dynamics and diversity of*
634 *human antibody responses to H5N1 vaccination.* Cell Rep, 2021. **34**(4): p. 108682.
635

Figure 1.

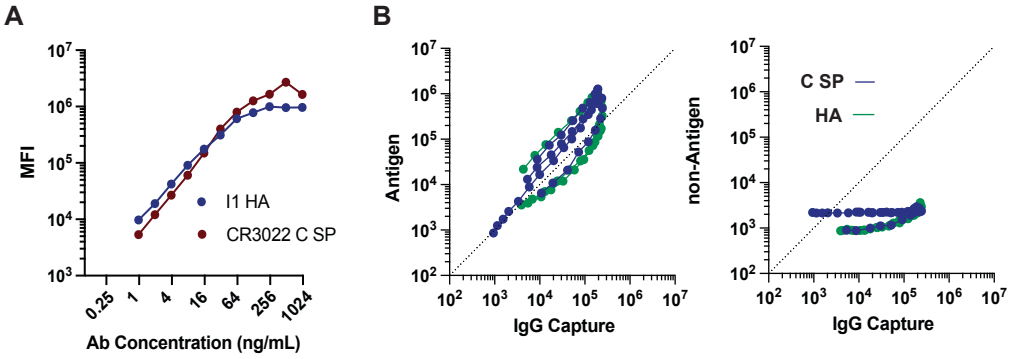
A
MFI
I1 HA
CR3022 C SP
Ab Concentration (ng/mL)
0.25
1
4
16
64
256
1024
B
Antigen
IgG Capture
non-Antigen
IgG Capture
C SP
HA

Figure 2.

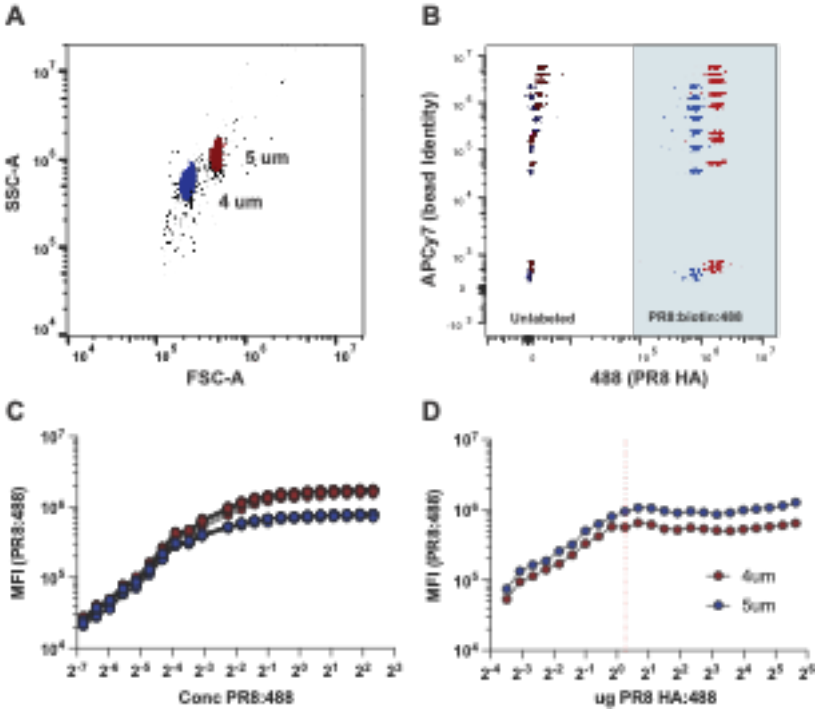
A
SSC-A
FSC-A
5 um
4 um
B
APCy7 (bead Identity)
488 (PR8 HA)
Unlabeled
PR8:biotin:488
C
MFI (PR8:488)
Conc PR8:488
D
MFI (PR8:488)
ug PR8 HA:488
4um
5um

Figure 3.

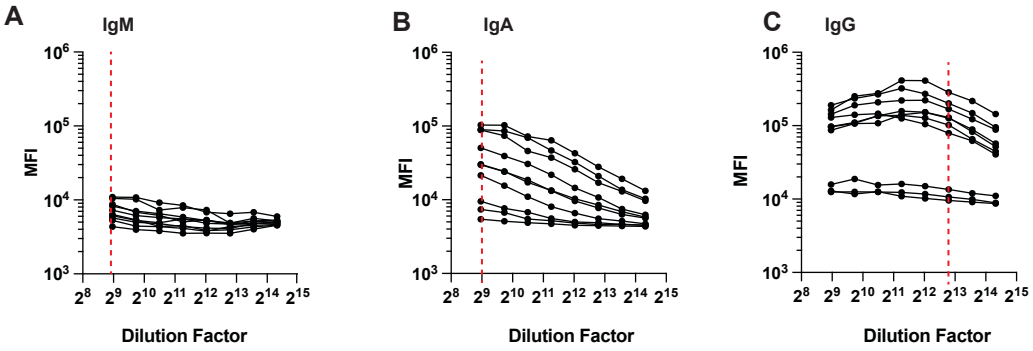
A
IgM
B
IgA
C
IgG
MFI
10^6
10^5
10^4
10^3
2^8 2^9 2^{10} 2^{11} 2^{12} 2^{13} 2^{14} 2^{15}
Dilution Factor

Figure 4.

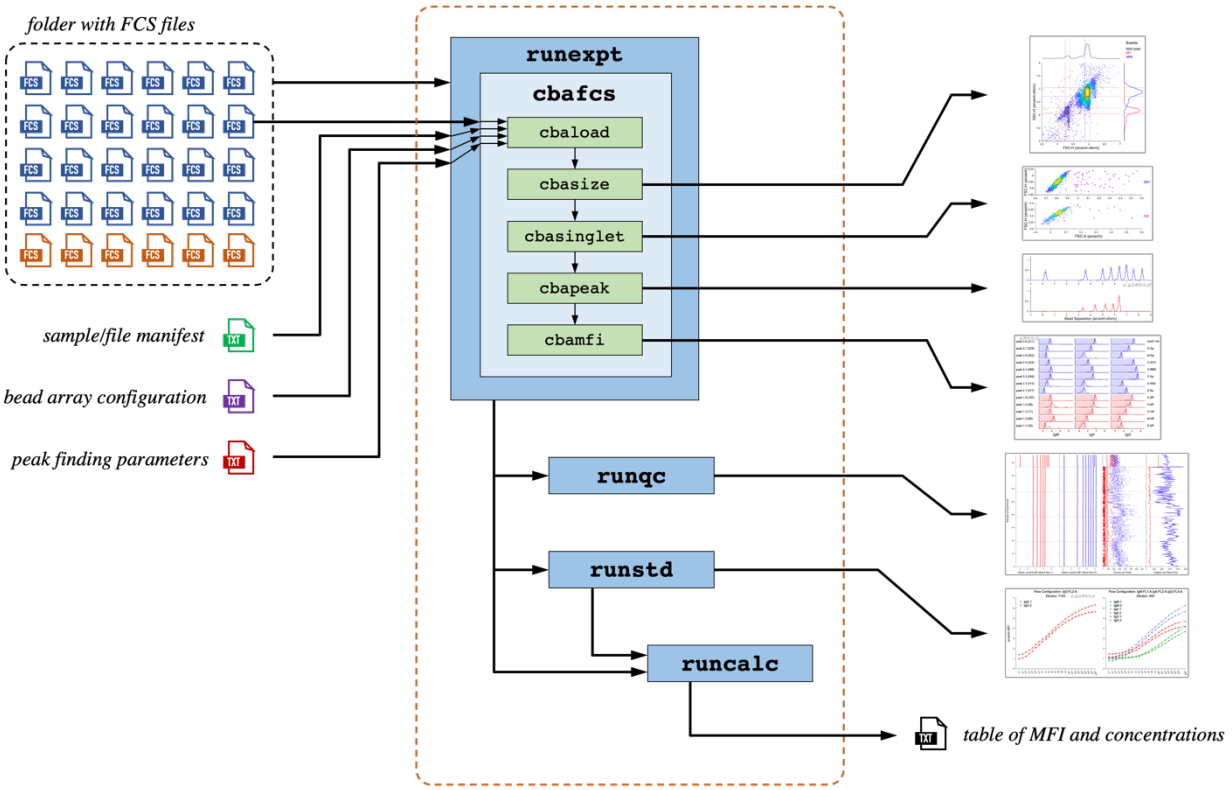
folder with FCS files
sample/file manifest
bead array configuration
peak finding parameters
runexpt
cbafcs
cbaload
cbasize
cbasinglet
cbapeak
cbamfi
runqc
runstd
runcalc
table of MFI and concentrations

Figure 5.

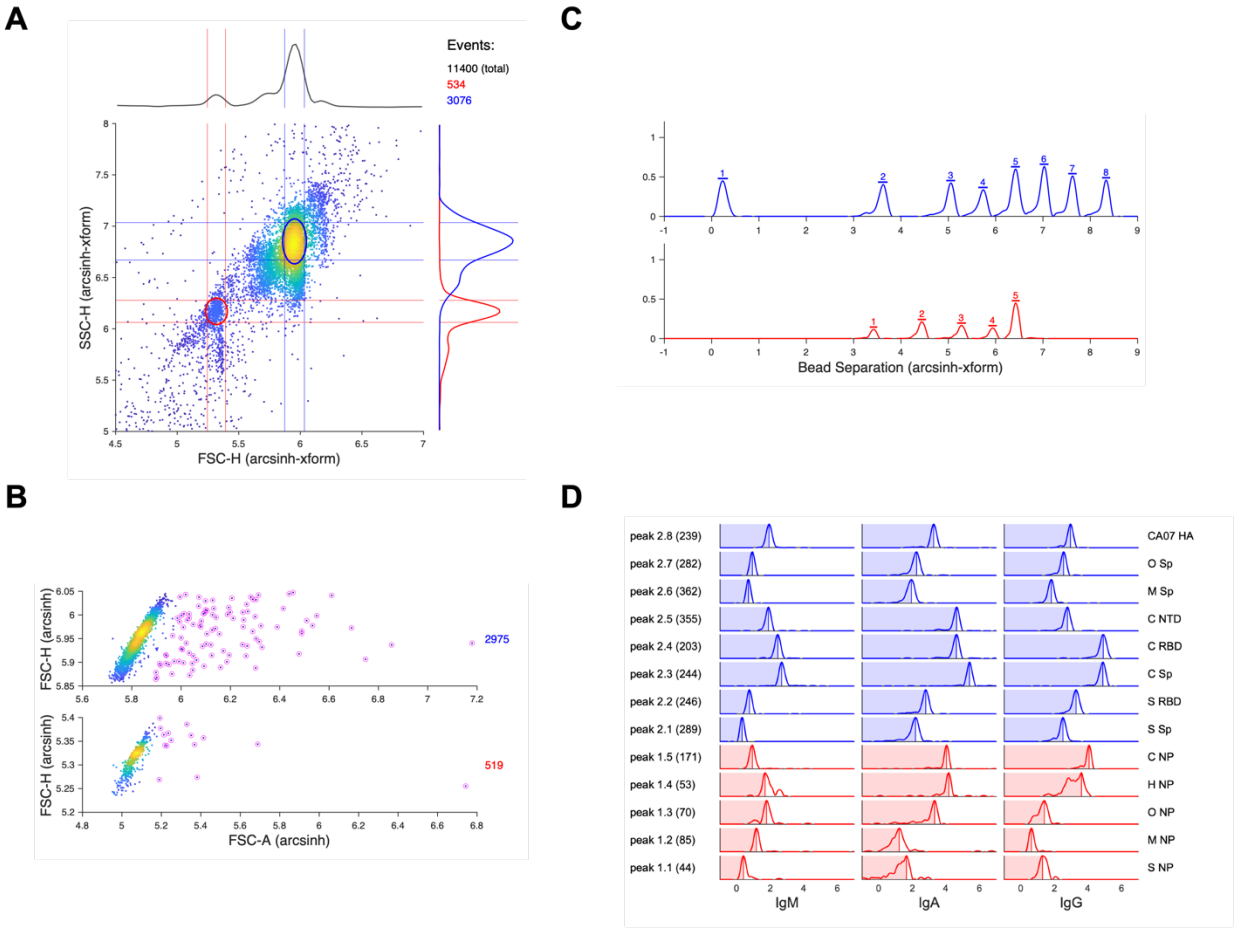
A
Events:
11400 (total)
534
3076
SSC-H (arcsinh-xform)
FSC-H (arcsinh-xform)
C
Bead Separation (arcsinh-xform)
B
FSC-H (arcsinh)
FSC-A (arcsinh)
2975
519
D
peak 2.8 (239)
peak 2.7 (282)
peak 2.6 (362)
peak 2.5 (355)
peak 2.4 (203)
peak 2.3 (244)
peak 2.2 (246)
peak 2.1 (289)
peak 1.5 (171)
peak 1.4 (53)
peak 1.3 (70)
peak 1.2 (85)
peak 1.1 (44)
CA07 HA
O Sp
M Sp
C NTD
C RBD
C Sp
S RBD
S Sp
C NP
H NP
O NP
M NP
S NP
IgM
IgA
IgG

Figure 6.

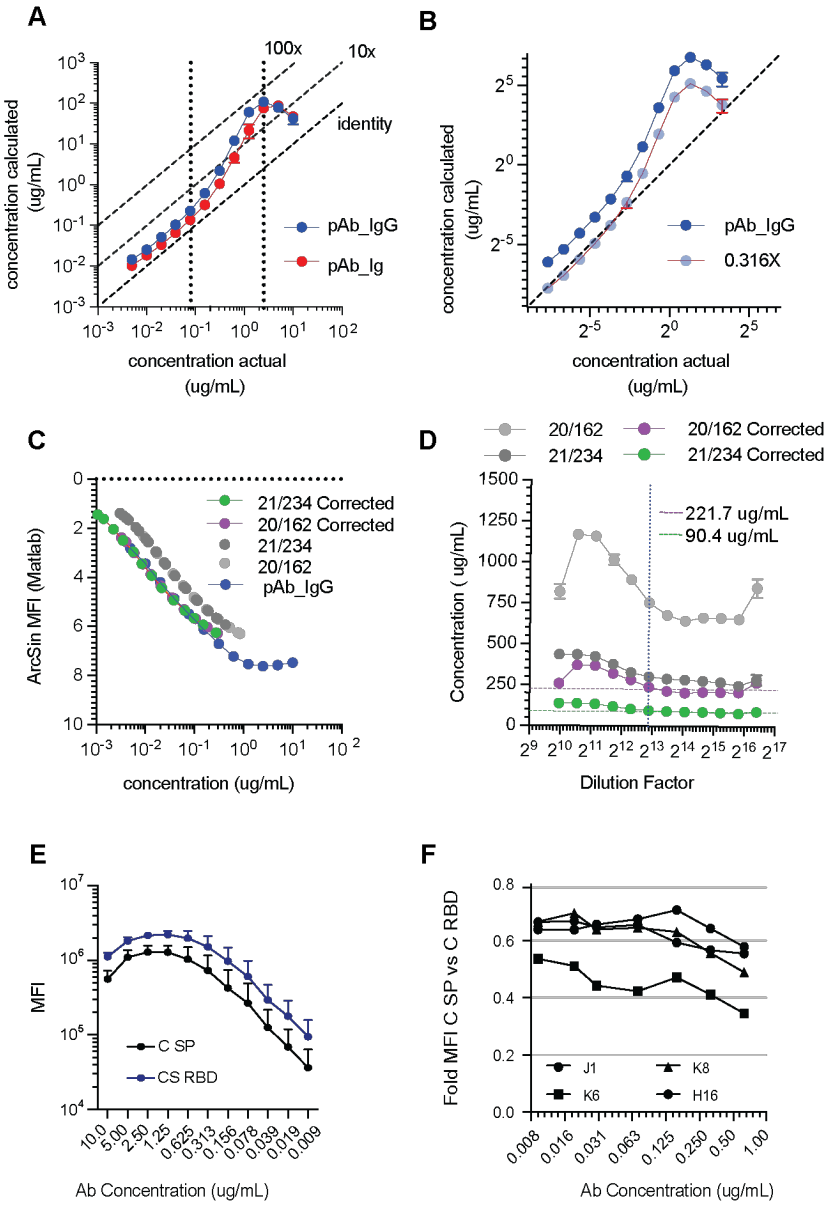
A
100x
10x
identity
pAb_IgG
pAb_Ig
concentration calculated (ug/mL)
concentration actual (ug/mL)
B
pAb_IgG
0.316X
concentration calculated (ug/mL)
concentration actual (ug/mL)
C
21/234 Corrected
20/162 Corrected
21/234
20/162
pAb_IgG
ArcSin MFI (Matlab)
concentration (ug/mL)
D
20/162
20/162 Corrected
21/234
21/234 Corrected
221.7 ug/mL
90.4 ug/mL
Concentration (ug/mL)
Dilution Factor
E
C SP
CS RBD
MFI
Ab Concentration (ug/mL)
F
J1
K8
K6
H16
Fold MFI C SP vs C RBD
Ab Concentration (ug/mL)

Figure 7.

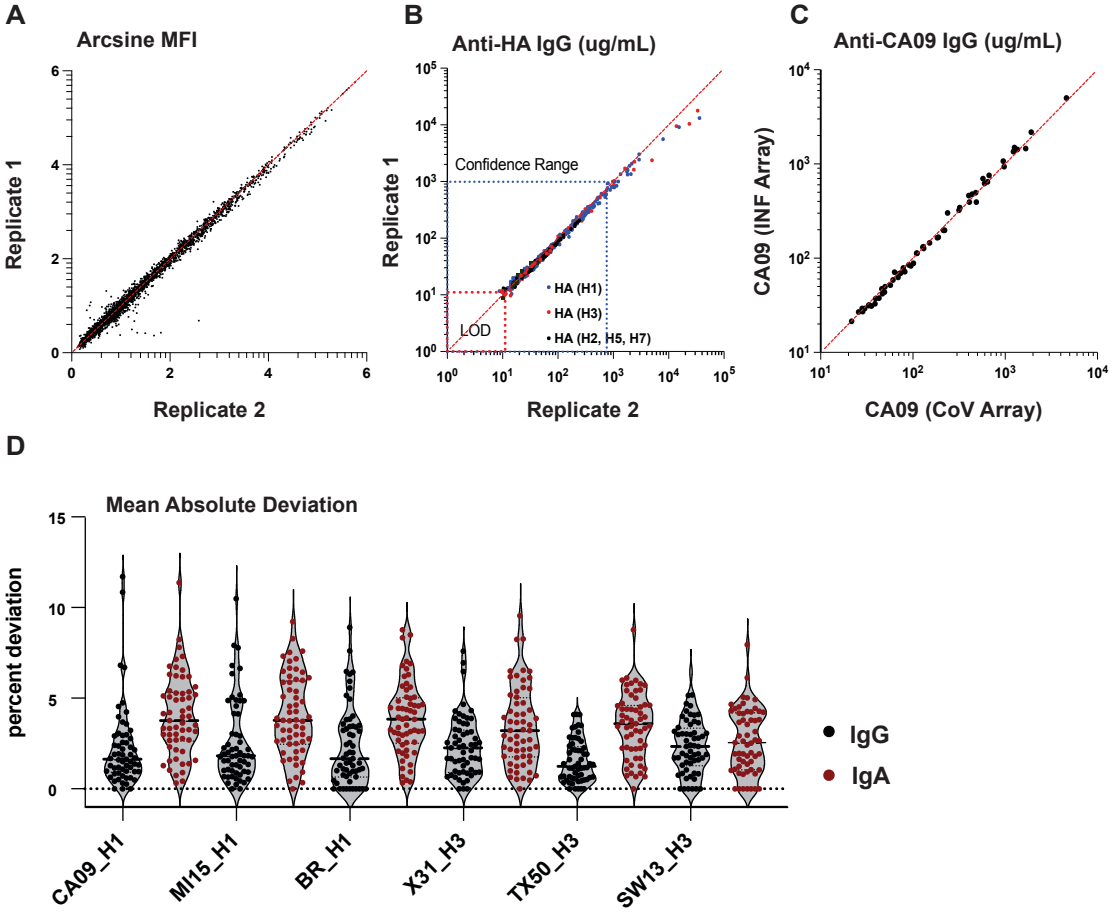
A
Arcsine MFI
Replicate 1
Replicate 2
B
Anti-HA IgG (ug/mL)
Confidence Range
LOD
HA (H1)
HA (H3)
HA (H2, H5, H7)
Replicate 1
Replicate 2
C
Anti-CA09 IgG (ug/mL)
CA09 (INF Array)
CA09 (CoV Array)
D
Mean Absolute Deviation
percent deviation
CA09_H1
MI15_H1
BR_H1
X31_H3
TX50_H3
SW13_H3
IgG
IgA

Figure 8.

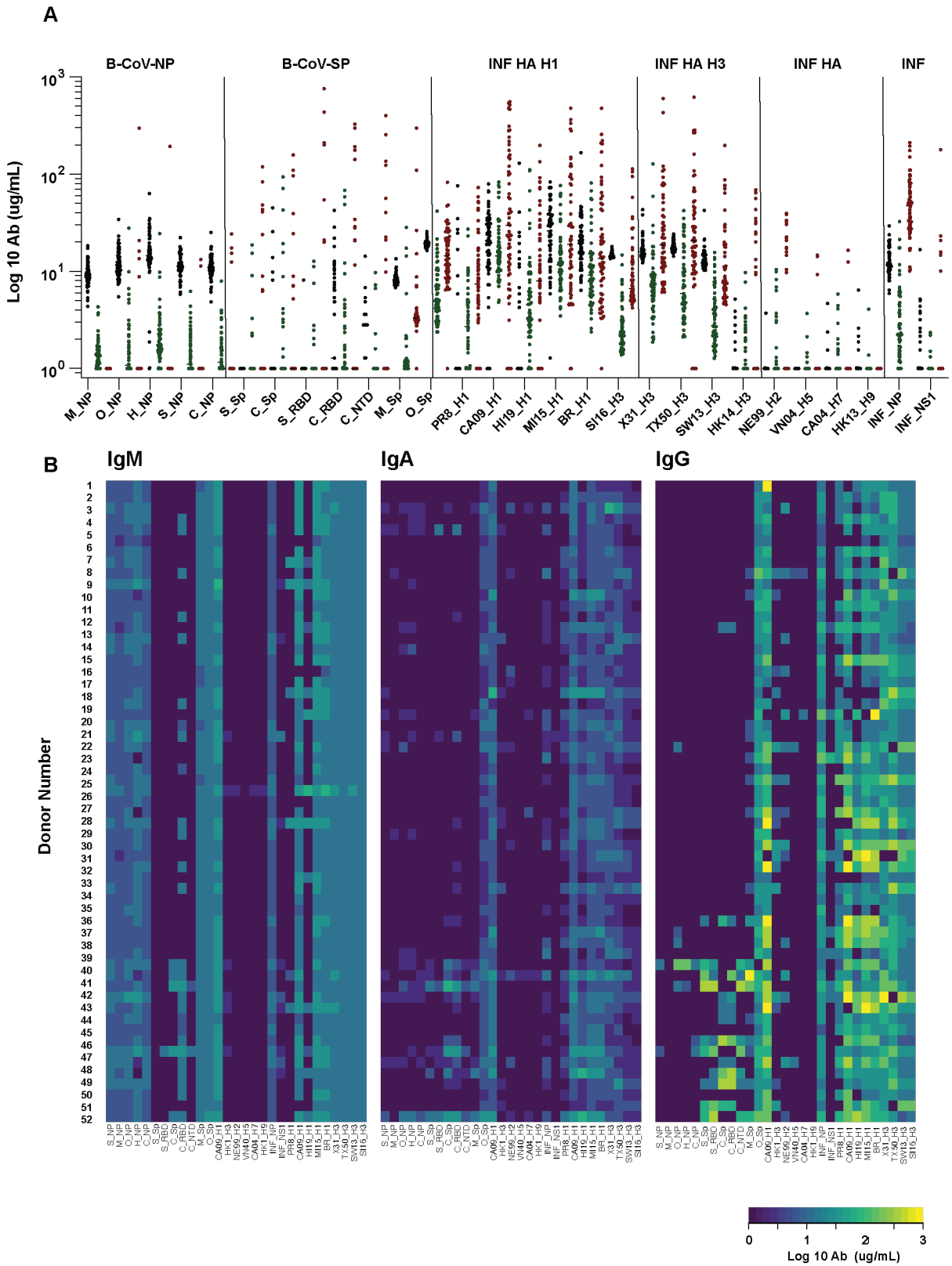
A
B-CoV-NP
B-CoV-SP
INF HA H1
INF HA H3
INF HA
INF
Log 10 Ab (ug/mL)
M_NP
O_NP
H_NP
S_NP
C_NP
S_Sp
C_Sp
S_RBD
C_RBD
C_NTD
M_Sp
O_Sp
PR8_H1
CA09_H1
HI19_H1
MI15_H1
BR_H1
SI16_H3
X31_H3
TX50_H3
SW13_H3
HK14_H3
NE99_H2
VN04_H5
CA04_H7
HK13_H9
INF_NP
INF_NS1
B
IgM
IgA
IgG
Donor Number
Log 10 Ab (ug/mL)

Figure 9.

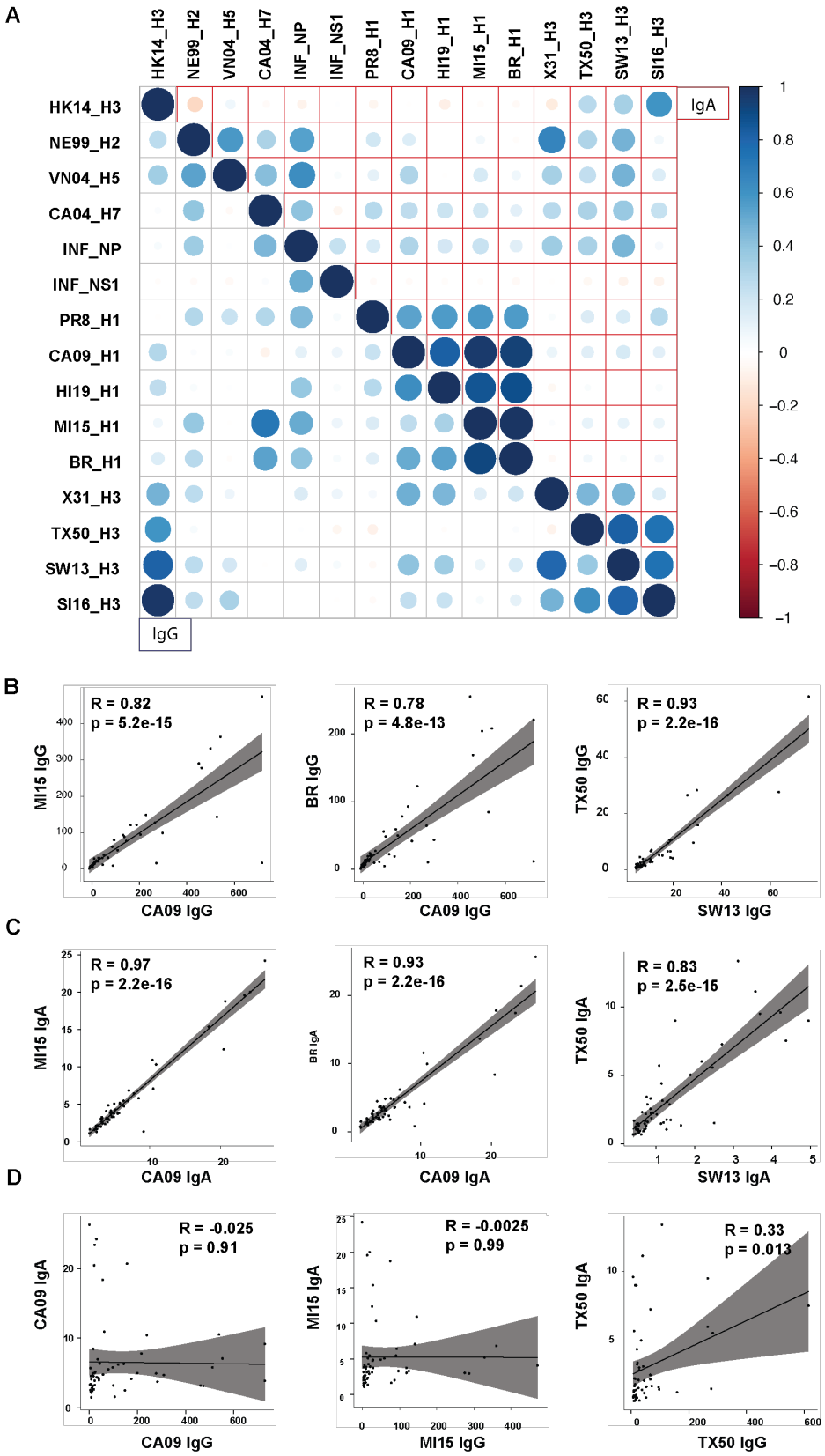
A
HK14_H3
NE99_H2
VN04_H5
CA04_H7
INF_NP
INF_NS1
PR8_H1
CA09_H1
HI19_H1
MI15_H1
BR_H1
X31_H3
TX50_H3
SW13_H3
SI16_H3
IgA
IgG
1
0.8
0.6
0.4
0.2
0
−0.2
−0.4
−0.6
−0.8
−1
B
R = 0.82
p = 5.2e-15
MI15 IgG
CA09 IgG
R = 0.78
p = 4.8e-13
BR IgG
CA09 IgG
R = 0.93
p = 2.2e-16
TX50 IgG
SW13 IgG
C
R = 0.97
p = 2.2e-16
MI15 IgA
CA09 IgA
R = 0.93
p = 2.2e-16
BR IgA
CA09 IgA
R = 0.83
p = 2.5e-15
TX50 IgA
SW13 IgA
D
R = -0.025
p = 0.91
CA09 IgA
CA09 IgG
R = -0.0025
p = 0.99
MI15 IgA
MI15 IgG
R = 0.33
p = 0.013
TX50 IgA
TX50 IgG

Table 1.

β-CoV			
4um-2	S NP	Sars-CoV-1 Nucleocapsid Protein	AAP13445.1
4um-3	M NP	MERS Nucleocapsid Protein	P_009047211.1
4um-4	O NP	OC43 Nucleocapsid Protein	KR055606.1
4um-5	H NP	HKU1 Nucleocapsid Protein	Q5MQC6.1
4um-6	C NP	Sars-CoV-2 Nucleocapsid Protein	QHD43423
5uM-1	S SP	Sars-CoV-1 Spike ectodomain	AAX16192.1
5uM-2	S RBD	Sars-CoV-1 Receptor binding domain	AAX16192.1
5uM-3	C SP	Sars-CoV-2 Spike ectodomain	QHD43416.1
5uM-4	C RBD	Sars-CoV-2 Receptor binding domain	QHD43416.1
5uM-5	C NTD	Sars-CoV-2 N-Terminal domain	QHD43416.1
5uM-6	M SP	MERS Spike ectodomain	AKI29255.1
5uM-7	O SP	OC43 Spike ectodomain	AAT84362.1
5uM-8	H SP	HKU1 Spike ectodomain	Q5MQD0.1
5uM-9	CA09	Influenza HA (H1)	NC_026433.1
Influenza			
Peak #	**Antigen**	**Antigen description**	**Protein Accession #**
5uM-1	PR8	Influenza HA (H1)	MH785011.1
5uM-2	CA09	Influenza HA (H1)	NC_026433.1
5uM-3	Hawaii2019	Influenza HA (H1)	MN976432.1
5uM-4	MICH15	Influenza HA (H1)	MK622940.1
5uM-5	Brisbane	Influenza HA (H1)	MN569031.1
5uM-6	X31	Influenza HA (H3)	DQ874876.1
5uM-7	TX50	Influenza HA (H3)	KC892952.1
5uM-8	SW13	Influenza HA (H3)	EPI543739
5uM-9	SING2016	Influenza HA (H3)	EPI2053182
4um-2	HK2014	Influenza HA (H3)	AKS48059.1
4um-3	NETH1999	Influenza HA (H2)	CY122252.1
4um-4	VN2004	Influenza HA (H5)	HM006759.1
4um-5	CAN04	Influenza HA (H7)	CY015013.1
4um-6	HongKong2013	Influenza HA (H9)	NAEPI498037
4um-7	INF NP	Influenza Nucleocapsid protein	NCAP_I34A1
4um-8	INF NS1	Influenza Non-structural protein	AAA43536

Figure legends

Figure 1. Dilution curves of antigen-specific antibodies. **A.** Plots of the MFI of beads coated with either CA09 HA or C SP and as a function of the concentration of the indicated mAb. **B**. Plots of the MFI of IgG capture beads and HA (green) or C SP (blue) coated beads simultaneously stained with dilutions of HA or C SP reactive Abs. Curves from the cognate antigen (left panel) or non-cognate antigen (right panel) are shown.

Figure 2. Array generation and loading controls. A. Forward and side scatter histograms for differentiating the indicated size particle. **B.** Flow cytometric histogram of the array constituents before (left, unshaded) and following incubation with biotinylated / alexa488 PR8 HA (right, shaded). **C.** MFI of each array constituent stained with the indicated concentration of PR8 HA:biotin:488. **D.** MFI of the indicated beads stained with increasing amount of PR8 HA:biotin:488 per 1e5 particles. Amount at which beads become saturated is indicated by the vertical red dashed line.

Figure 3. Optimal assay serum dilution determination. MFI of CS SP Beads stained with serial dilutions of human serum from COVID convalescent patients visualized with secondaries reactive to the indicated human Ig isotype. Serum Dilutions selected to assay for each isotype are indicated by red dashed lines.

Figure 4. Schematic of automated software modules. Software components are shown within red dashed box. Green boxes are modules that perform a single element of processing. The light blue box is a program that processes a single FCS file to extract transformed MFI data for all features in the assay. The darker blue box represents a wrapper to batch process many FCS files (represented in black dashed box) and annotates whether an FCS file is a normal sample (blue) or a standard control sample (orange). A sample manifest is used in batch mode to provide sample metadata. Additionally, a bead array configuration file and a peak finding parameter file contain parameters that describe association of beads with proteins and settings applied to each file. After the program is run in batch mode, there are modules for bead gate quality assessment, construction of standard curves and back-calculation to concentration units. When running for an individual file, figures can be generated for diagnostic purposes (right).

Figure 5. Raw FCS data processing steps. All intensity data is hyperbolic arcsin transformed. A. Forward scatter vs. side scatter to identify densities of events associated with multiple bead sizes. Red and blue ovals are gates for 4um and 5um beads, respectively. B. Density-based clustering on forward scatter height vs. area to identify outliers, or non-singlets for each bead size gate. C. Identification of peaks on the specified bead channel for each bead size after non-singlets filtered out. Line segments above each peak are individual bead gates. D. Hyperbolic arcsine MFI intensity plots on the secondary isotype channels (columns of plots) for each bead size/peak gate (rows of plots). For each row, number of beads per gate indicated in parentheses. Antigen features for this example panel are: C = SARS-CoV-2; S = SARS-CoV-1; M = MERS; O

= OC43; H = HKU-1; CA07 HA = California 07 influenza hemagglutinin; Sp = spike protein; RBD = receptor binding domain; NP = nuclear protein; NTD = n-terminal domain.

Figure 6. Quantitated polyvalency and C SP subunit corrections. A. Extrapolated concentration of anti- CS SP pAb and pIgG plotted against the known concentration. **B**. Calculated polyvalency correction factor for anti-CS SP pAb IgG. Fold difference in MFI between CS SP and CS RBD across the linear range of dilutions is shown. **C**. Hyperbolic arcsine transformed MFI values derived from the array plotted against known concentration of anti-CS SP pAb and uncorrected values derived from the indicated NISBC standards. Corrected values were generated by linear scaling of the extrapolated concentrations. **D.** Extrapolated anti-CS SP antibody concentrations (before and after polyvalent correction) of the indicated NISBC standards. Dashed lines indicated the high confidence Ab concentration of the indicated standards. **E.** Mean MFI of the CS SP coated (black) or C RBD coated (blue) beads stained the indicated concentrations of anti-CS RBD reactive rAbs. The resulting mean and SD of the MFIs of CS SP and CS RBD are shown. **F.** The ratio of the MFI of CS SP to CS RBD of the indicated anti-CS RBD rAbs at the indicated concentration.

Figure 7. Assay reproducibility. **A.** Scatter plot of the ArcSin MFI of each bead for all samples for two independent measurements of the CCHI U19 cohort serum. The values of the two replicates are plotted pairwise. **B**. Extrapolated antibody concentration for the two replicates ploted pairwise for the indicated HA antigens. **C**. Scatter plot of the derived concentration of Ab reactive with CA09 HA derived from the COVID and INF arrays. **D**. Mean absolute deviation for each data point of two replicates across the two replicates for the indicated antigens and Ab isotypes.

Figure 8. The reactivity profiles of 96 sera samples toward the full β-Cov and INF arrays. **A.** The concentration of IgM (black), IgA (green), and IgG (red) reactive with the indicated antigen as measured by the Coba and INF array. **B.** Heatmap of the log10 Ab concentration (ug/mL) for the indicated antigen. Each row corresponds to an individual serum, and each column corresponds to the indicated antigen, IgM, IgA, and IgG are shown.

Figure 9. Correlation of Ab levels for HA antigens in the array. A. The pairwise Pearson correlation coefficient for either IgG (lower left) or IgA (upper right) of Ab levels for each antigen in the INF Array. **B.** Scatter profiles of antibody levels toward the indicated H1 and H3 hemagglutinins for the 59 samples in the cohort.

Table 1. List of antigens used to generate the Inf and β-CoV antigen Arrays.
The size and peak number of each array element is listed, with the biotinylated recombinant protein loaded to generate the two arrays. The protein accession numbers are provided.